



Contents lists available at ScienceDirect

Catalysis Today

journal homepage: [www.elsevier.com/locate/cattod](http://www.elsevier.com/locate/cattod)



## Influence of the metallic content on Pt-Ir/Nb<sub>2</sub>O<sub>5</sub> catalysts for decalin selective ring opening

Viviana M. Benitez<sup>a</sup>, Simone P. de Lima<sup>b</sup>, Maria do Carmo Rangel<sup>b</sup>, Doris Ruiz<sup>c</sup>,  
Patricio Reyes<sup>c</sup>, Carlos L. Pieck<sup>a,\*</sup>

<sup>a</sup> Instituto de Investigaciones en Catálisis y Petroquímica (INCAPE) (FIQ-UNL, CONICET), Colectora Ruta Nac. No 168 Km. 0, Paraje El Pozo, 3000, Santa Fe, Argentina

<sup>b</sup> GECCAT Grupo de Estudos em Cinética e Catálise, Instituto de Química, Universidade Federal da Bahia, Rua Barão de Geremoabo, 147. Campus Universitário de Ondina. 40.170-115, Salvador, Bahia, Brazil

<sup>c</sup> Departamento de Físico Química, Facultad de Ciencias Químicas, Universidad de Concepción, Casilla 160-C, Concepción, Chile

### ARTICLE INFO

#### Article history:

Received 9 May 2016

Received in revised form 24 August 2016

Accepted 3 October 2016

Available online xxx

#### Keywords:

Decalin

Platinum

Iridium

Niobium

SRO

### ABSTRACT

Ring opening of naphthenic rings on Pt-Ir catalysts supported on Nb<sub>2</sub>O<sub>5</sub> was studied in this work. The catalysts were prepared by impregnation. In the case of the bimetallic catalyst, the total metallic load was kept constant while varying the individual quantity of impregnated Ir and Pt. The samples were characterized by transmission electron microscopy, X-ray diffraction, X-ray photoelectron spectroscopy, N<sub>2</sub> sorption, NH<sub>3</sub> TPD and model reactions (cyclohexane dehydrogenation and cyclopentane hydrogenolysis). The decalin ring opening capacity of the catalysts was evaluated. Monometallic Ir and Pt catalysts as well as bimetallic catalysts were active towards cyclohexane dehydrogenation and cyclopentane hydrogenolysis. Regarding the bimetallic catalysts, an increase on the Pt content promoted the cyclohexane dehydrogenation while hindering the hydrogenolytic activity. In the selective ring opening of decalin, the bimetallic catalysts presented activities comparable to the monometallic catalysts. Nonetheless, Ir(0.3%)/Nb<sub>2</sub>O<sub>5</sub> catalyst presented the highest selectivity towards ring opening products with the lowest selectivity towards dehydrogenated products.

© 2016 Elsevier B.V. All rights reserved.

### 1. Introduction

Light Cycle Oil (LCO), a low value by product of the Fluid Catalytic Cracking (FCC) process, has been proposed as a potential source of diesel. However, diesel has to comply with certain quality requirements regarding cetane index, aromatic content, sulfur content, etc. to be used in motors due to numerous environmental regulations [1,2]. Although LCO contains hydrocarbons on the diesel range, its aromatic content (particulate material forming compounds) is very high and it is necessary to transform them into other hydrocarbons. It has been reported that LCO contains from 0.2 to 2 wt% of sulfur and between 48 and 69% of polyaromatics, yielding a cetane index (CI) between 22 and 25. The European norms in January 2009 demand an upper limit of 10 ppm of S and 11% of polyaromatics with a minimum cetane index of 51 [3]. The elimination of S and N compounds can be carried out by hydrotreatment technologies

[4–6] which can also be useful to hydrogenate aromatics. However, a CI increase by conversion of polyaromatics to naphthenics is not enough since the CI of naphthenic compounds is pretty low [7,8]. The ring opening of at least one of the naphthenic rings is necessary to achieve an adequate CI. Selective ring opening occurs when the molecular weight remains almost constant since only internal C–C bonds on the naphthenic rings are broken, whereas a non-selective breaking of the external C–C bonds will lead to a variety of products with a lower overall molecular weight. This is clearly a difficult task, since endocyclic cracking of naphthenes is less thermodynamically favored than acyclic and exocyclic cracking reactions due to entropy considerations [9].

Calemma et al. [10] point out that three principal families of solid catalysts are usually distinguished for the cleavage of C–C bonds: (i) monofunctional acidic catalysts, (ii) bifunctional catalysts containing both Brønsted acid and metal sites and (iii) monofunctional metal catalysts. Onyestyák et al. [11] and McVicker et al. [12] have thoroughly studied the opening of alkyl-substituted mononaphthene rings in the C<sub>6</sub>–C<sub>10</sub> range and have proven the good selectivity of Ir catalysts towards the aperture of five membered rings. The ring opening (RO) rate over Ir decreases significantly as the alkylsubsti-

\* Corresponding author at: INCAPE Colectora Ruta Nac. No 168 Km. 0, Paraje El Pozo, 3000, Santa Fe, Argentina.

E-mail address: [pieck@fiq.unl.edu.ar](mailto:pieck@fiq.unl.edu.ar) (C.L. Pieck).

<http://dx.doi.org/10.1016/j.cattod.2016.10.004>

0920-5861/© 2016 Elsevier B.V. All rights reserved.

tution degree increases and is directly proportional to the number of secondary carbons. Contrary to Ir, Pt is found to be more active towards the breaking of C–C bonds on substituted carbons. However, the RO rate on Pt is sensitive to the cis/trans configuration on methyl-substituted cyclopentanes and diminishes proportionally to the concentration of the trans isomer. Cardoso et al. [13] found evidence of a bifunctional mechanism in the hydroconversion of decalin over Pt/Beta zeolite catalysts, since the selectivity depends on the metal/acid function balance.

In acid catalysts, contrary to metal-assisted ring opening reactions, it is thought that C<sub>6</sub>–C<sub>7</sub> naphthenic RO occurs over the Brønsted acid sites and is initiated by protolytic cracking, followed by chained reactions involving the carbenium ion formed [14,15]. Kubicka et al. [16,17] found that acidity has an important role on the selectivity of bicyclic naphthenic ring opening.

Current experiences show that the more active and convenient catalysts are those based on supported Ir, since they have a very low contribution towards the rupture of exocyclic chains. Nonetheless, the most convenient product distribution occurs over five-membered rings instead of six-membered rings. Two recent studies thoroughly examined the reaction paths for the hydroconversion of decalin on non-acidic supports such as  $\gamma$ -Al<sub>2</sub>O<sub>3</sub> [18] and SiO<sub>2</sub> [10]. Depending on the Ir content (between 0.5 and 2.6%), the decalin conversion starts between 250 and 350 °C with no skeletal isomerization. In perspective, silica-supported Pt catalysts require temperatures around 350–400 °C producing larger quantities of dehydrogenated products [18]. Furthermore, Vicerich et al. [19] studied the SRO of decalin at 325 °C and found that monometallic Pt and Ir catalysts supported on SiO<sub>2</sub> produces only dehydrogenated products. Recently, the experimental use of SRO coupled with Catalytic Assisted Sulfur Traps (CAST), has shown that the operation of a SRO-CAST process is superior to the traditional hydrocracking process to upgrade refinery cuts [20]. As a disadvantage, hydrogenolysis is extremely sensitive to sulfur poisoning. Hence, SRO reactions require a complete removal of S, including desulphurization of beta-dibenzothiophenes.

Open literature shows that acidic monofunctional catalysts suffer from coke deposition deactivation during decalin ring opening caused by the formation of significant quantities of hydrocarbons with more than 10 carbon atoms at high conversions while the formation of RO products is low, around 10% [21].

In this work, ring opening was studied on metallic catalysts of noble metals (Pt, Ir) deposited on Nb<sub>2</sub>O<sub>5</sub>. The objective was to produce active catalysts, stable and selective towards SRO of cycloalkanes with one or various rings. Model molecules used were decalin, cyclohexane and cyclopentane.

## 2. Experimental

### 2.1. Preparation of bimetallic Ir-Pt catalysts supported on Nb<sub>2</sub>O<sub>5</sub>

The niobium oxide used as support was obtained by calcination of hydrated niobium pentoxide (niobic acid HY-340, supplied by CBMM, Brazil) at 450 °C. The catalysts were prepared by impregnation of the support (Nb<sub>2</sub>O<sub>5</sub>) with metal precursor solutions (H<sub>2</sub>IrCl<sub>6</sub> and H<sub>2</sub>PtCl<sub>6</sub>). The total metallic load was 1 wt% and the catalysts were prepared with a molar ratio Ir/Pt of 0.5, 1 and 2. First, 1.5 cm<sup>3</sup> g<sup>-1</sup> of a solution of HNO<sub>3</sub> (2 M) was added to the support in order to favor the homogenous distribution of metals inside the support particles. The solution was left 1 h to rest. Then, the adequate amount of hexachloroiridic and/or hexachloroplatinic acid was added in order to reach a 1 wt% metal load and the desired Ir/Pt ratio. The system was left to rest for 1 h again to allow for a uniform distribution of the metals. In order to evaporate the solvent (water), the solid was put on a water bath at 70 °C under mild

stirring until a dry powder was obtained. Later, it was further dried in a stove at 120 °C for 12 h. Finally, the samples were calcined at 450 °C, for 3 h and reduced with hydrogen at 500 °C, for 4 h.

### 2.2. Preparation of monometallic Ir and Pt catalysts supported on Nb<sub>2</sub>O<sub>5</sub>

The same procedure described for the bimetallic catalysts was used. Monometallic catalysts with 0.3, 0.5 and 0.7 wt% of Pt or Ir were prepared.

### 2.3. Evaluation of the Pt and Ir content

The composition of the metal phase was determined by Inductively Coupled Plasma-Optical Emission Spectroscopy (ICP-OES, Perkin Elmer, Optima 2100 DV) after digestion in an acid solution and dilution.

### 2.4. Specific surface area

Nitrogen adsorption isotherms (–196 °C) were recorded on an automatic Micromeritics ASAP-2020 apparatus. Prior to the adsorption experiments, the samples were outgassed at 140 °C, for 2 h. BET areas were computed from the adsorption isotherms (0.05 < P/P<sub>0</sub> < 0.27). A value of 0.164 nm<sup>2</sup> was assumed for the cross section of the adsorbed N<sub>2</sub> molecule at –196 °C.

### 2.5. X-ray diffraction (XRD)

The analysis were performed at room temperature using a Shimadzu XRD-7000 diffractometer with monochromated CuK  $\alpha$  radiation ( $\lambda = 1.54 \text{ \AA}$ ) operated at 40 kV and 30 mA. Diffractograms were recorded in the 2 $\theta$  range from 10 to 80° at a resolution of 0.05° with a scanning speed of 2° min<sup>-1</sup>, using a nickel filter. Samples were analyzed in powder form.

### 2.6. Transmission electron microscopy (TEM)

Micrographs were obtained in a Jeol JEM 1200 EXII microscope. Each supported catalysts was ground in an Agatha mortar and dispersed in ethanol. Diluted drops of these dispersions were placed on a 150 mesh copper grid with carbon. The micrographs were obtained in both bright and dark fields.

The dispersion was estimated as the ratio between the theoretical minimum particle diameter and the apparent particle diameter measured by TEM, according to the method of Kubika [22].

### 2.7. X-Ray photoelectron spectroscopy (XPS)

Before the XPS analyses were performed, the solids were treated in situ with a H<sub>2</sub>:Ar mixture at 400 °C and then degassed to a residual pressure of 5.9 × 10<sup>-7</sup> Pa. For each sample the analyzed regions of the spectrum were those containing the signals due to the Pt 4f<sub>7/2</sub> and 4f<sub>5/2</sub>, Ir 4f<sub>7/2</sub> and 4f<sub>5/2</sub> and Nb 3d<sub>5/2</sub> and 3d<sub>3/2</sub> core levels. The binding energy of carbon (C1s = 284.8 eV) was used for the calibration of XPS data. Spectrum peak areas were calculated by integration. Peaks were fitted to a 70/30 sum of Gaussian and Lorentzian functions and the background was considered to be of the Shirley type. More technical details can be found in a previous report [23].

### 2.8. Temperature programmed desorption of NH<sub>3</sub>

A Micromeritics TPD/TPR 2900 model fitted with a TCD detector was used for the acidity measurements by NH<sub>3</sub>-TPD. Samples were reduced for an hour at 300 °C (50 cm<sup>3</sup> min<sup>-1</sup> of H<sub>2</sub>). After reduction,

samples were cooled on helium ( $45 \text{ cm}^3 \text{ min}^{-1}$ ) to  $110^\circ\text{C}$ , then saturated with gaseous ammonia injected through a calibrated loop under a stabilized He flow for 30 min. After cooling at room temperature, the temperature programmed desorption began, heating the solid from 30 up to  $770^\circ\text{C}$ , under a heating rate of  $10^\circ\text{C min}^{-1}$ , using helium as a carrier gas ( $45 \text{ cm}^3 \text{ min}^{-1}$ ).

### 2.9. Cyclopentane hydrogenolysis

the catalysts were reduced for 1 h at  $500^\circ\text{C}$  in  $\text{H}_2$  ( $60 \text{ cm}^3 \text{ min}^{-1}$ ) before reaction. They were then cooled in  $\text{H}_2$  to the reaction temperature ( $250^\circ\text{C}$ ). The other conditions were: catalyst mass = 150 mg, pressure = 0.1 MPa,  $\text{H}_2$  flow rate =  $40 \text{ cm}^3 \text{ min}^{-1}$ , cyclopentane flow rate =  $0.483 \text{ cm}^3 \text{ h}^{-1}$ . The products were analyzed chromatographically in a Varian 3400 CX chromatograph equipped with a capillary column (Phenomenex ZB-1) and a conventional FID.

### 2.10. Cyclohexane dehydrogenation

the reaction was performed in a glass reactor under the following conditions: catalyst mass = 100 mg, temperature =  $300^\circ\text{C}$ , pressure = 0.1 MPa, hydrogen flow rate =  $80 \text{ cm}^3 \text{ min}^{-1}$ , cyclohexane flow rate =  $1.61 \text{ cm}^3 \text{ h}^{-1}$ . Before the reaction was started, the catalysts were treated in  $\text{H}_2$  ( $60 \text{ cm}^3 \text{ min}^{-1}$ ,  $300^\circ\text{C}$ , 1 h). The products were analyzed by capillary GC as described before.

### 2.11. Selective ring opening (SRO) of decalin

all SRO experiments were performed in an autoclave-type stirred stainless steel reactor. The reaction conditions were: temperature =  $350^\circ\text{C}$ , hydrogen pressure = 3 MPa, stirring rate = 1360 rpm, decalin volume =  $25 \text{ cm}^3$ , catalyst load = 1 g, catalyst particle size = 35–80 meshes. Decalin with a trans/cis ratio of 1.63 (i.e. 37.5% of the cis isomer) was used. After a few minutes, it was found that the attrition action of the stirrer reduced the catalyst to a powdery slurry that would mostly pass through a 200 meshes sieve after drying. Given the particle size and the high stirring rate, diffusional limitations were assumed to be eliminated. This was further confirmed by a calculated Weisz-Prater modulus of 0.06 (much lower than 1). At the end of the experiments, a sample was taken and analyzed in a Varian 3400 CX gas chromatograph equipped with a capillary column (Phenomenex ZB-5) and a FID.

Previous product identification studies were performed by GC–MS in a Saturno 2000 mass spectrometer coupled to a GC Varian 380 using the same GC column.

### 2.12. Results and discussion

For all samples, ICP-OES results are in close agreement with the expected theoretical metal contents. Table 1 shows the specific surface areas of the different catalysts. It can be seen that all catalysts present the same specific surface area due to the low metal load.

The XRD patterns of the support and catalysts are shown in Fig. 1. As can be seen, the support (calcined at  $450^\circ\text{C}$ ) showed a large and broad peak at about  $2\Theta = 25^\circ$  and the absence of any crystallite peaks of  $\text{Nb}_2\text{O}_5$  indicated that the catalysts were amorphous or that the corresponding  $\text{Nb}_2\text{O}_5$  crystallites were too small to be detected. Moreover, the characteristic peaks due to TT- $\text{Nb}_2\text{O}_5$  (pseudo-hexagonal), T- $\text{Nb}_2\text{O}_5$  (orthorhombic) and H- $\text{Nb}_2\text{O}_5$  (monoclinic) phases [24] were not observed, supporting the amorphous structure of the support. The amorphous phase of the support is in agreement with Braga et al. [25] and Koi and Weissman [26] who reported that the phase transition occurs at a higher temperature. The monometallic Pt and Ir catalysts, as well as the bimetallic catalysts (calcined at  $450^\circ\text{C}$  and reduced at  $500^\circ\text{C}$ ) showed also at larger broad peak at

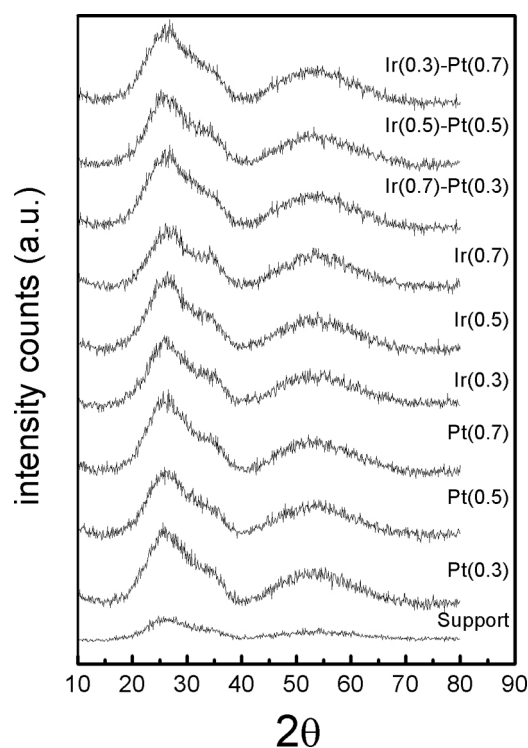


Fig. 1. XRD pattern of the support and all studied catalysts.

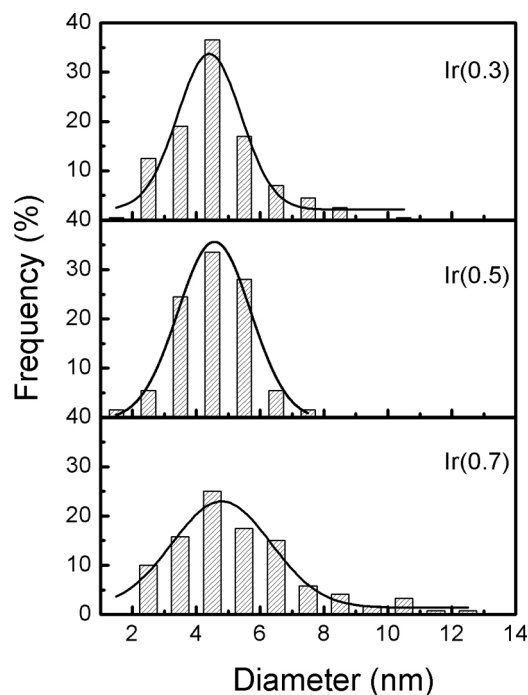


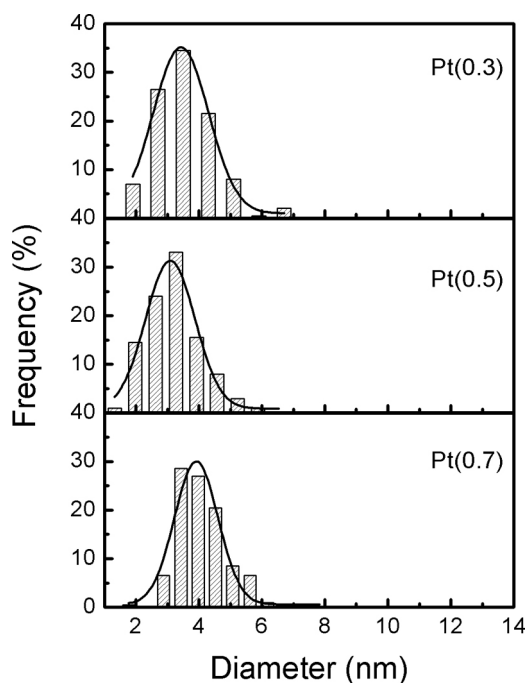
Fig. 2. Particle size distributions obtained by TEM for monometallic Ir catalysts.

$2\Theta = 25^\circ$ . These samples show no diffraction peaks of either Pt or Ir under metallic or oxide form, which reveals that metal particles species on the samples surface are amorphous or very small and highly dispersed within the matrix. However, the higher height of the peak zone between  $20$  and  $40^\circ$  and  $40$  to  $70^\circ$  may indicate an incipient formation of some niobium oxides nanocrystals [27].

Figs. 2 to 4 show the particle size distributions obtained by TEM for the monometallic Ir and Pt catalysts and for the bimetallic catalysts. As can be seen in Fig. 2, an increase in the Ir content leads

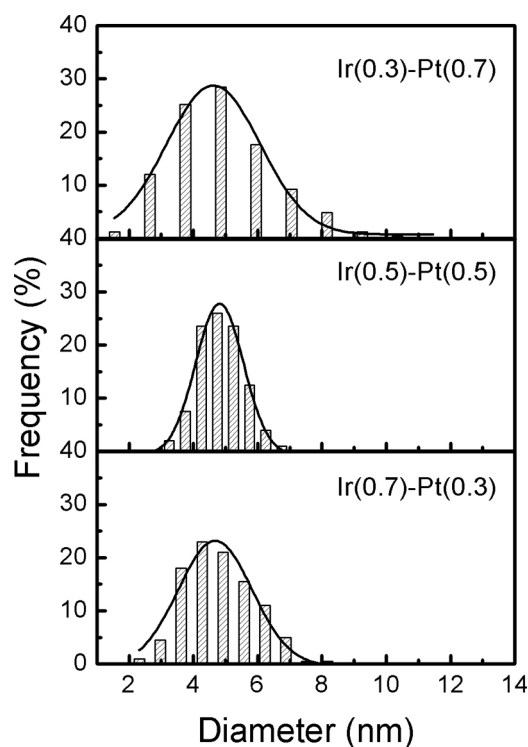
**Table 1**  
Specific surface area, and mean particle size and metal dispersion values obtained by TEM.

Catalyst	Specific surface area (m <sup>2</sup> g <sup>-1</sup> )	Mean diameter TEM (nm)	Metal dispersion (%)
Pt(0.3)	80	3.4 ± 1.7	28
Pt(0.5)	80	3.1 ± 1.5	30
Pt(0.7)	84	3.9 ± 1.4	24
Ir(0.3)	74	4.4 ± 2.0	21
Ir(0.5)	73	4.3 ± 1.6	22
Ir(0.7)	80	4.8 ± 3.1	19
Ir(0.3)-Pt(0.7)	80	4.6 ± 2.9	
Ir(0.5)-Pt(0.5)	82	4.8 ± 1.5	
Ir(0.7)-Pt(0.3)	80	4.7 ± 2.3	

**Fig. 3.** Particle size distributions obtained by TEM for monometallic Pt catalysts.

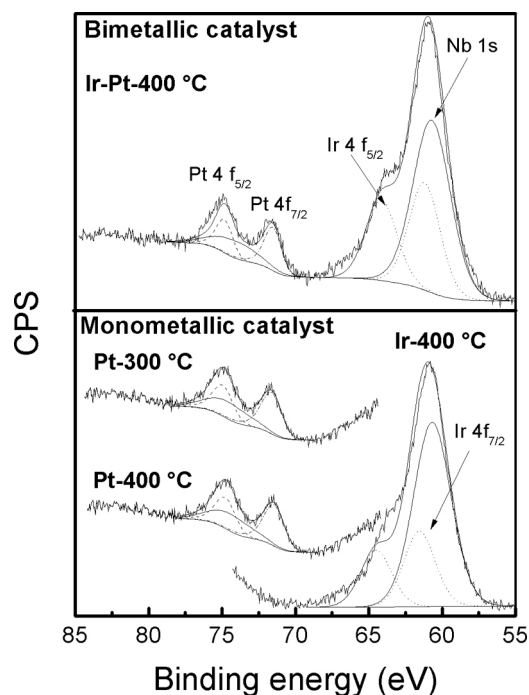
to an increase of the mean Ir particle size for monometallic catalysts. Furthermore, the catalyst with the highest Ir load presents the broadest particle size distribution, including seldom very large particles. In the case of monometallic Pt (Fig. 3) an increase on the metal load produces a slight increase on the mean particle size. Fig. 4 shows that bimetallic catalysts present different particle size distributions depending on their composition, the Ir (0.3)-Pt (0.7) sample showing the broadest distribution. On the other hand, the Ir(0.5)-Pt(0.5) catalyst shows a narrow particle size distribution. Table 1 displays the mean particle size of all studied catalysts. It is concluded that Ir and bimetallic catalysts present bigger particles than Pt catalysts. These particle size distributions resulted in the highest metal dispersion for platinum monometallic catalysts and similar metal dispersions for the other samples.

Fig. 5 represents the XPS spectra of Pt(0.3)/Nb<sub>2</sub>O<sub>5</sub> and Ir(0.3)/Nb<sub>2</sub>O<sub>5</sub> monometallic catalysts as well as the spectrum of Ir(0.7)-Pt(0.3)/Nb<sub>2</sub>O<sub>5</sub> catalysts. The binding energy (BE) of the Pt 4f<sub>7/2</sub> and Pt 4f<sub>5/2</sub> are at 71.5 and 74.8, respectively, in good agreement with the BE for metallic Pt (71.6 eV) [28]. Unfortunately, the signal due to the energy loss of Nb (obtained on Nb<sub>2</sub>O<sub>5</sub> without Pt) does disturb these signals. However, it is possible to see that both BEs are identical for the monometallic Pt catalyst previously reduced at 300 and 400 °C. Moreover, the Pt/Nb ratio was equal in both samples and equal to the Pt/Nb bulk ratio. Equal Pt/Nb ratios obtained by XPS and chemical analysis (bulk) were reported by

**Fig. 4.** Particle size distributions obtained by TEM for bimetallic Ir-Pt catalysts.

Guerrero et al. [29]. These results confirm that subsequent treatments with hydrogen at lower temperature do not modify the electronic properties of Pt. The XPS spectrum of monometallic Ir/Nb<sub>2</sub>O<sub>5</sub> catalysts shows the Ir 4f<sub>7/2</sub> and Ir 4f<sub>5/2</sub> at 61.6 and 64.5 eV which is attributed to metallic Ir [30]. The Ir/Nb ratio was higher than the bulk ratio probably due to the lower Ir dispersion. However, it must be taken into account that these bands are strongly influenced by Nb 4s (60.6 eV) which adds uncertainty to the Ir/Nb ratio. In the case of bimetallic catalysts, the Ir 4f peaks are shifted to a lower BE while the Pt 4f is shifted to a higher BE compared with the monometallic catalyst. The shift is very small because both metals have very similar electronegativities (2.28 and 2.20 Pauling units). This fact suggests the formation of a bimetallic Ir-Pt alloy or simply the existence of interactions between Pt and Ir [30]. The small shift to higher BEs of the Ir 4f signal and the slight shift to lower BEs of the Pt 4f were also found by Chen and Chen [31] and were attributed to electronic interactions between the Pt and Ir atomic orbitals. Table 2 shows a summary of the main XPS results. As a conclusion, in all cases Pt and Ir are in the metallic state and there is an interaction between Pt and Ir on bimetallic catalysts.

Before analyzing the TPD results, it is important to point out that the acid sites of the catalysts are mainly attributed to the support but can be influenced by the metal deposition. Probably, the



**Fig. 5.** XPS of 4f levels of Pt and Ir in monometallic Pt(0.3) and Ir(0.3) catalysts and bimetallic Ir(0.7)-Pt(0.3) catalysts. Samples reduced at 300 °C or 400 °C before XPS analysis.

**Table 2**

Ir/Nb and Pt/Nb ratio obtained by XPS and binding energy of Pt 4f and Ir 4f of the monometallic Pt and Ir and bimetallic Ir-Pt catalyst.

Catalyst	Pt 4f <sub>7/2</sub>	Pt 4f <sub>5/2</sub>	Ir 4f <sub>7/2</sub>	Ir 4f <sub>5/2</sub>	Pt/Nb	Ir/Nb
Pt(0.3)-300 °C	71.5	74.8	–	–	0.002	–
Pt(0.3)-400 °C	71.5	74.8	–	–	0.002	–
Ir(0.3)-400 °C	–	–	61.6	64.5	–	0.006
Ir(0.7)-Pt(0.3)-400 °C	71.7	75.0	61.1	64.0	0.002	0.009

adsorption of Pt and Ir during the impregnation step occurs on the stronger acid sites of the support. The precursors used were H<sub>2</sub>PtCl<sub>6</sub> and H<sub>2</sub>IrCl<sub>6</sub> which are hydrolyzed into PtCl<sub>6</sub><sup>2-</sup> and IrCl<sub>6</sub><sup>2-</sup>. These anions are adsorbed on the Brønsted acid sites of the support, decreasing the acidity of the support. Once reduced, Pt and Ir are in metallic state and have no influence on the acidity. Also, it must be taken into account that both metal precursors include chlorine, which is an important promoter of the acidity and which remains on the support. Studying alumina, Gates et al. [32] proposed that the acidity of an OH group is strengthened by the inductive effect exerted by a Cl<sup>-</sup> ion adjacent to the OH group. This model agrees with the observations of Tanaka and Ogasawara [33,34].

Fig. 6 shows the NH<sub>3</sub> TPD profiles obtained while the total acidity and acid sites distribution of the monometallic and bimetallic series catalysts can be found on Table 3. Ammonia TPD allows classifying acid sites as weak, medium or strong depending on the NH<sub>3</sub> desorption temperature [35]. Logically, higher desorption temperatures correspond to stronger acid sites. It can be seen in Table 3 that the addition of Ir, Pt or both metals together decreases the total acidity of the support between 5 and 35%. Moreover, it is observed in Table 3 that for the monometallic Ir series the total acidity increases with the Ir content. In addition, the apparition of a shoulder between 140 and 250 °C which increases at higher Ir contents can be observed in Fig. 6, which implies an increase on the number of medium acidity sites. Fig. 6 shows that monometallic Pt catalysts display a broad desorption peak at about 80 °C and another one at 170 °C which shifts slightly to higher temperatures

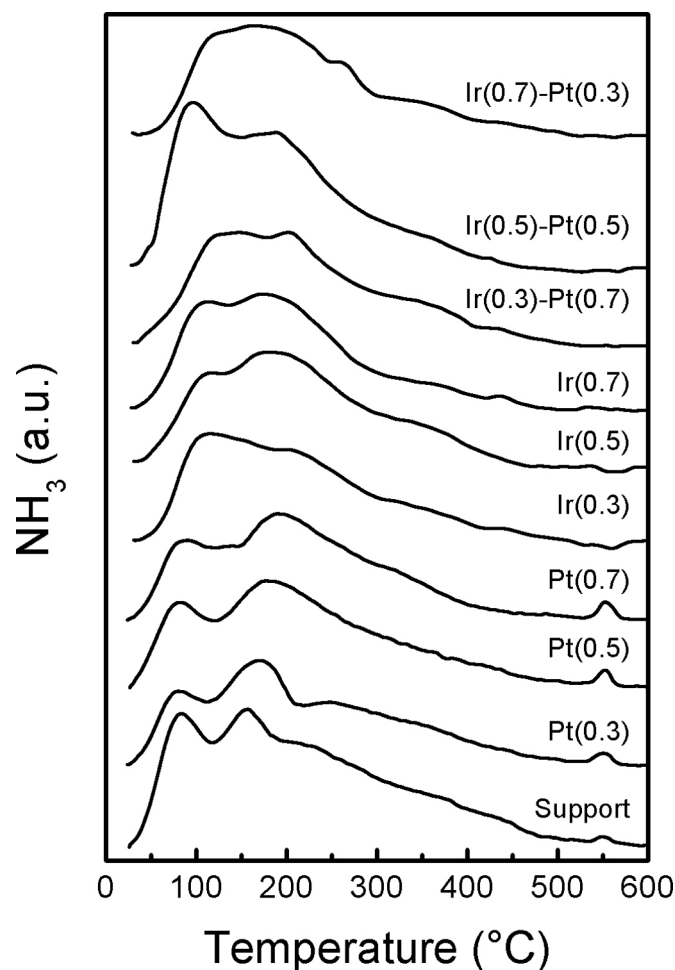


**Fig. 6.** Ammonia TPD curves for support and all studied catalysts.

with an increase on the Pt content. Monometallic Pt(0.5) and Pt(0.7) catalysts have similar total acidity (Table 3) and higher acidity than the monometallic Pt(0.3) catalyst. Increasing the Pt content leads to an increase in the amount of moderate acid sites while the amount of strong acid sites decreases (Table 3). In the case of bimetallic catalysts, Table 3 shows that maximum total acidity is found on the Ir(0.5)-Pt(0.5) catalyst. However, Fig. 6 shows that this higher acidity is caused by an increase of weakly acid sites (with a desorption temperature about 88 °C). Moreover, the results in Table 3 put in evidence that the higher total acidity of the Ir(0.5)-Pt(0.5) catalyst is due to an increased amount of weak acid sites and to a lesser extent to the increase of moderate acid sites.

Cyclohexane (CH) dehydrogenation and cyclopentane hydrogenolysis conversion values for all catalysts can be found on Table 4. The catalysts achieved 100% selectivity towards benzene and did not show any deactivation during dehydrogenation (1 h). For this reason, Table 4 reports only the mean conversion values (12 points). On the other hand, the catalysts produced a myriad of products such as *n*-pentane, propane, ethane, methane, etc. and were deactivated rapidly by coke deposition during hydrogenolysis. Therefore, the reported data corresponds to 5 min after reaction start. Both reactions occur exclusively through a monofunctional mechanism catalyzed by metallic sites on the catalyst under the studied conditions. CH dehydrogenation is a non-demanding reaction and hence its reaction rate is considered proportional to the number of exposed surface metallic atoms. On the contrary, CP hydrogenolysis requires a particular metallic ensemble, i.e. it is a reaction sensible to structure [36–38].

**Table 3**  
Total acidity and acid sites distribution ( $\mu\text{mol NH}_3 \text{ g}^{-1}$ ) determined by ammonia temperature programmed desorption.

Catalyst	Acid sites distribution			Total acidity
	Weak( $T < 150^\circ\text{C}$ )	Moderate( $150 < T < 300^\circ\text{C}$ )	Strong( $T > 300^\circ\text{C}$ )	
Support	134.7	173.7	94.6	403
Pt(0.3)	81.7	124.8	65.5	272
Pt(0.5)	87.5	144.6	64.9	297
Pt(0.7)	82.1	145.6	57.3	285
Ir(0.3)	79.5	119.9	60.6	260
Ir(0.5)	78.6	153.3	64.1	296
Ir(0.7)	118.2	157.9	69.9	346
Ir(0.3)-Pt(0.7)	75.1	135.5	59.4	270
Ir(0.5)-Pt(0.5)	152.5	173.5	57.0	383
Ir(0.7)-Pt(0.3)	76.3	146.8	55.9	279

**Table 4**  
CH dehydrogenation and CP hydrogenolysis conversion results.

Catalyst	Conversion (%)		CP/CH*100
	CH	CP	
Pt(0.3)	45.0	1.8	4.0
Pt(0.5)	58.0	2.4	4.1
Pt(0.7)	71.0	2.6	3.7
Ir(0.3)	6.2	2.2	35.5
Ir(0.5)	6.6	3.2	48.5
Ir(0.7)	7.8	4.9	62.8
Ir(0.3)-Pt(0.7)	38.0	1.7	4.5
Ir(0.5)-Pt(0.5)	27.0	3.6	13.3
Ir(0.7)-Pt(0.3)	20.0	5.4	27.0

CP/CH: conversion of cyclopentane/conversion of cyclohexane.

It is important to point out before analyzing the metal activity that niobium oxides have been reported to exhibit a pronounced effect on the metal, being a typical strong metal support interaction (SMSI) oxide [39–42]. Ir and Pt could be blocked by this SMSI phenomenon, since the metal activity is strongly affected as they are covered by suboxide species formed by support reduction.

As stated, after metal impregnation the catalysts were activated by calcination ( $450^\circ\text{C}$ , 4 h) and reduction ( $500^\circ\text{C}$ , 4 h). Strong metal-support interaction (SMSI) effects occurring during the reduction step have been reported [30,43–48]. Therefore, the SMSI phenomenon is expected to occur during the reduction step of the activation of the catalysts. Some researchers reported that the metallic properties of the metal are restored after oxidation at  $400^\circ\text{C}$  followed by reduction at low temperature [46,49], while others researchers reported that the oxidation must be carried out at higher temperature ( $500^\circ\text{C}$ ) in oxygen flow in order to reverse the phenomenon [50,51]. The catalysts were not submitted to an oxidative treatment after activation; they were put into contact with the atmospheric air at room temperature. As a consequence, the migration of niobia oxides or SMSI effects produced during reduction at  $500^\circ\text{C}$  were unaltered. Furthermore, the reduction temperatures used before the reaction tests are unable to modify any SMSI effects produced at higher temperatures on the previous steps. In order to obtain additional experimental evidence, some selected catalysts were tested again using the cyclopentane reaction with a previous reduction at  $300^\circ\text{C}$  and  $350^\circ\text{C}$ . As expected (results not shown) the reduction temperature does not show any influence on cyclopentane conversions.

Table 4 shows that monometallic Pt catalysts are more active than Ir catalysts towards CH dehydrogenation. This behavior was expected given the superior dehydrogenation activity of Pt compared to Ir [52,53]. Moreover, the result is in agreement with the higher metallic dispersion of Pt measured by TEM (in Table 1, Figs. 2 and 3). The CH dehydrogenation rate increases with the Pt or Ir content for the monometallic catalysts given the increased

amount of metal atoms on the surface, since the dispersion remains practically constant (Table 1).

Bimetallic catalysts present an intermediate behavior, being their activity more influenced by the Pt content, i.e., the activity increases with the Pt/Ir ratio. It is important to note that bimetallic catalysts have lower dehydrogenation activity than the monometallic catalysts. This behavior shows that Pt is blocked by Ir which has a lower dehydrogenation activity. This effect could be due to geometric (blocking) or electronic factors (modification of the Pt electronic density due to interaction with Ir) [54].

Regarding the hydrogenolytic activity, it can be observed from Table 4 that monometallic Ir catalysts are more active towards CP hydrogenolysis than their Pt counterparts. Since this is a demanding reaction, the highest activity would be expected on the catalysts with the lower metallic dispersion. However, this effect could be compensated by a reduced effective number of ensembles. It means that as the dispersion decreases, the activity of the ensembles increases but they become scarce. It should be noted that the variation of the hydrogenolytic activity is greater for the monometallic Ir series, probably due to formation of larger crystals at high Ir loads as found by TEM for the Ir(0.7) catalyst. Regarding the bimetallic catalysts, CP conversion increases with Ir content given the higher hydrogenolytic activity of Ir over Pt [53].

Although the SMSI phenomenon could affect the properties of the catalysts, analyzing the CP/CH ratio can still be useful to determine the demanding/non-demanding reaction ratio on the remaining unblocked sites. It can be seen in Table 4 that Ir catalysts had higher CP/CH ratios than Pt catalysts, while this ratio increased along with the Ir/Pt ratio in the case of bimetallic catalysts. These results were expected since Ir is more hydrogenolytic and presents less dehydrogenating activity than Pt [52,53]. Pt catalysts only showed little variation due to the small particle size changes. The Ir series had great increases in the CP/CH ratio since hydrogenation activity remained almost constant while the hydrogenolytic activity increased threefold at higher Ir loads. The higher CP/CH ratio of the Ir(0.7) catalyst could be attributed to the large particles (larger than 9 nm) reported in Fig. 2. At a higher Ir content, a lower SMSI effect must be considered.

The SRO of naphthenic compounds such as decalin should lead to the breakage of an endocyclic C–C bond, causing a reduction on the number of ring structures and keeping a constant number of carbon atoms throughout the reaction. However, this breakage can occur in the substituted C–C bond or in the alkyl-substituted groups, depending on the metal and support. Decalin SRO produces a complex mixture with more than 200 compounds. These products were classified according to criteria used in previous works [55]. The reaction products were classified as: cracking products ( $\text{C}_1\text{--}\text{C}_9$ ), ring opening products (RO), ring contraction products and dehydrogenated compounds such as naphthalene.

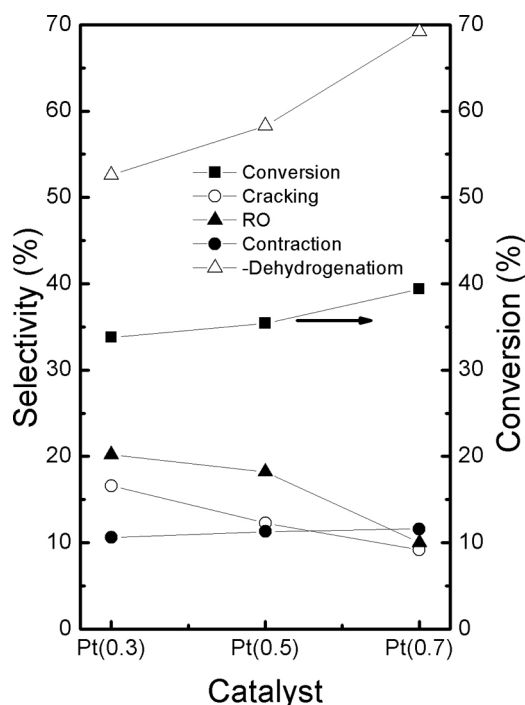


Fig. 7. Decalin conversion and selectivity towards cracking, ring opening (RO), ring contraction and dehydrogenation products obtained after 6 h of reaction for monometallic Pt catalysts.

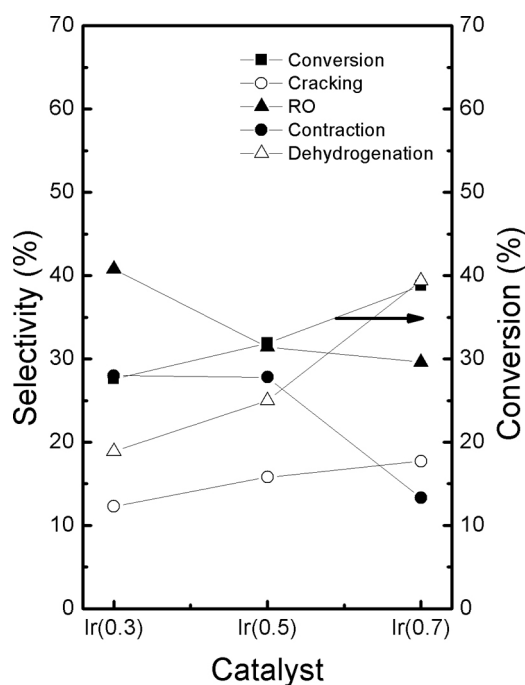


Fig. 8. Decalin conversion and selectivity levels towards cracking, ring opening (RO), ring contraction and dehydrogenation products obtained after 6 h of reaction for monometallic Ir catalysts.

Figs. 7 to 9 present the decalin conversion values obtained after 6 h at 350 °C and 35 atm, as well as the selectivity towards different reaction products. It can be seen in Fig. 7 that conversion increases as the Pt content increases for monometallic catalysts. These results are in agreement with previous works [10,56] but contrary to the values reported by Cardoso et al. [13]. They have found that the overall reaction rate was unrelated to the hydrogenation activity

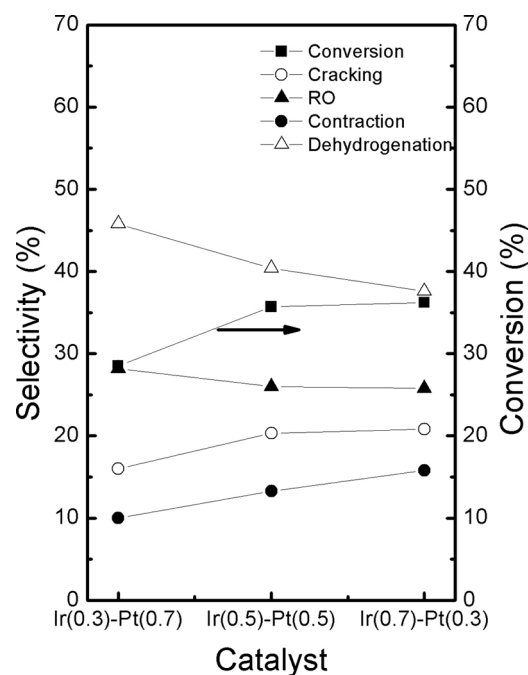


Fig. 9. Decalin conversion and selectivity levels towards cracking, ring opening (RO), ring contraction and dehydrogenation products obtained after 6 h of reaction for bimetallic Ir-Pt catalysts.

(metal content) of a Pt/Beta zeolite catalyst. The increase in decalin conversion with Pt content is in agreement with the increase of hydrogenolysis and dehydrogenation activities reported in Table 4. On the other hand, the selectivity towards RO and cracking products decreases with an increasing Pt load.

The ring contraction products are mostly unaffected by Pt content. Moreover, as expected by the CH dehydrogenation results (Table 4), the selectivity towards dehydrogenation products increases with increasing Pt loads. Overall, the increase in Pt content leads to higher selectivity to dehydrogenated products while it decreases the formation of ring opening and cracking products.

These results point out that Pt favors mostly dehydrogenation reactions due to its lower hydrogenolytic activity (Table 4). As a consequence, the selectivity towards RO products is low and even decreases as the Pt content increases. Considering that the formation of cracking products corresponds to a bifunctional mechanism where the controlling reaction step occurs over the acid function [57] it can be argued that its decrease is possibly caused by a decrease in the strong acid sites of the support at higher Pt loads (Table 3). On bifunctional catalysts, the acid function has been reported to promote the formation of intermediate carbenium ions, which isomerize into five membered rings that readily undergo subsequent ring opening on acid or metal sites [2]. Therefore, the poor performance of the Pt/Nb<sub>2</sub>O<sub>5</sub> series regarding decalin SRO could be due to the low hydrogenolytic activity of Pt. Under this conditions, the bifunctional mechanism towards RO products is hindered and the catalyst leads to the formation of dehydrogenation products (>50%). Hence, Pt/Nb<sub>2</sub>O<sub>5</sub> catalysts are poorly fitted for decalin SRO.

Decalin SRO over monometallic Ir catalysts shows an activity (conversion) slightly below that of their monometallic Pt catalyst counterparts (Fig. 7). Likewise, the activity increases according to the Ir load. However, Ir-based catalysts exhibited considerably less production of dehydrogenation products compared to Pt-based catalysts, as reported by Table 4, i.e., the higher conversion of Pt catalysts compared to Ir catalysts could be due to the higher amount of dehydrogenated products formed on those catalysts. Also, as for

the monometallic Pt catalysts, the selectivity to dehydrogenation products increases with Ir content in agreement with the results from cyclohexane dehydrogenation, as reported in Table 4. Cracking products are also favored at higher Ir loads, while RO products reach a maximum at 0.3 wt% of Ir. This increase in the generation of cracking products at higher Ir loads could correspond to an increase of the catalyst acidity (mainly the strong acid sites) [2,58] as reported in Table 3 and Fig. 6, as well as, an increase in the hydrogenolytic activity due to an increase in the Ir content (Table 4). The higher selectivity to RO products of the Ir(0.3) catalysts compared to other monometallic Ir catalysts could be due to its very low cyclohexane dehydrogenation activity combined with a low but comparatively higher hydrogenolytic activity. Under these conditions, RO products are generated by hydrogenolysis while the formation of dehydrogenated products is limited.

For bimetallic catalysts, Fig. 9 shows that the activity (conversion) was found to be close to those of the Pt and Ir catalysts. Moreover, the activity increases with the Ir/Pt ratio of the catalysts. It can be seen that an increase on the Pt load leads to a higher amount of dehydrogenation products in agreement with cyclohexane dehydrogenation results shown in Table 4, while the selectivity towards RO products slightly increases.

The generation rate of dehydrogenation products on bimetallic catalysts is between those of the monometallic catalysts, as expected. The cracking products can be attributed to Ir, since their production rate is proportional to the Ir load (i.e. it decreases with the Pt load). The amount of cracking products is also correlated to the acidity values reported on Table 3. It should be taken into account that cracking reactions are catalyzed by strong acid sites and to a lesser degree by the moderate acid sites. Since the highest acidity of the Ir(0.5)–Pt(0.5) catalyst is mainly caused by weak sites and in part by moderate acid sites (Fig. 6, Table 3), the formation of cracking products is unaffected.

The formation of ring contraction products is promoted by the acid sites of the catalyst. After that, they are transformed into ring opening products by the metal function of the catalyst [7]. Hence, the amount of ring contraction products depends on the balance between the formation rate by an acid-controlled step and the disappearance rate by dehydrogenation and ring opening. This fact makes it almost impossible to correlate their amount with any property of the catalyst. However, in the case of bimetallic catalysts, the amount of ring contraction products increases at high Ir loads.

It is interesting to compare the performance on decalin reaction of the monometallic catalyst using different supports. The conversion of decalin obtained for monometallic Pt and Ir catalysts was higher than the conversion obtained on Pt and Ir supported on Al<sub>2</sub>O<sub>3</sub> and TiO<sub>2</sub> but lower than the conversion obtained on Pt and Ir supported on zeolite [55,59]. These differences could be due to the acidity of the catalysts since higher activities are obtained on zeolites which present the highest acidity. The selectivity to RO products was also higher on the catalysts supported on zeolite showing the importance of acid sites in the reaction. This result supports the ring contraction from 6 to 5 carbon atoms (easier to open) as the first and rate-determinant reaction step as previously proposed [2,7].

### 3. Conclusions

Monometallic Ir and Pt catalysts supported on niobium oxide are active towards cyclohexane dehydrogenation and cyclopentane hydrogenolysis. The hydrogenolytic and dehydrogenation activity increases with the metal load for monometallic catalysts. In the case of cyclohexane, the highest activity was found for the monometallic Pt catalysts while Ir catalysts showed the highest

hydrogenolytic activity. Regarding bimetallic catalysts, an increase in the Pt/Ir ratio leads to an increase in the dehydrogenation activity and to a decrease in the hydrogenolytic activity attributable to the interactions between Pt and Ir. Decalin selective ring opening reaction tests show that monometallic Ir catalysts are more selective towards ring opening products. Pt addition increases the selectivity towards naphthalene and decreases the selectivity towards the desired ring opening products. This can be ascribed to the elevated dehydrogenation capacity of Pt. The highest selectivity towards ring opening products was shown by an Ir(0.3%)/Nb<sub>2</sub>O<sub>5</sub> catalyst.

### Acknowledgments

The authors acknowledge CIAM/CNPq for the financial contribution.

### References

- [1] J.J. Elliott, M.T. Melchior, Kirk-Othmer Encyclopedia of Chemical Technology, vol. 17, 3rd ed., John Wiley & Sons, Inc USA, 1982, pp. 119.
- [2] H. Du, C. Fairbridge, H. Yang, Z. Ring, Appl. Catal. A 294 (2005) 1–21.
- [3] R. Moraes, K. Thomas, S. Thomas, S. Van Donk, G. Grasso, J.P. Gilson, Marwan Houalla, J. Catal. 299 (2013) 30–43.
- [4] C. Song, X. Ma, Appl. Catal. B 41 (2003) 207–238.
- [5] Y. Yoshimura, H. Yasuda, T. Sato, N. Kijima, T. Kameoka, Appl. Catal. A 207 (2001) 303–307.
- [6] W. Qian, Y. Yoda, Y. Hirai, A. Ishihara, T. Kabe, Appl. Catal. A 184 (1999) 81–88.
- [7] M. Santikunaporn, J.E. Herrera, S. Jongpatiwut, D.E. Resasco, W.E. Alvarez, E.L. Sughrue, J. Catal. 228 (2004) 100–113.
- [8] B.H. Cooper, B.B.L. Donniss, Appl. Catal. A 137 (1996) 203–223.
- [9] J. Govindhakannan, K. Chandra Mouli, A. Phoenix, A.K. Fairbridge, Fuel 97 (2012) 400–410.
- [10] A. Haas, S. Rabl, M. Ferrari, V. Calemma, J. Weitkamp, Appl. Catal. A 425–426 (2012) 97–109.
- [11] G. Onyestyák, G. Pál-Borbély, H.K. Beyer, Appl. Catal. A 229 (2002) 65–74.
- [12] G.B. McVicker, M. Daage, M.S. Touvelle, C.W. Hudson, D.P. Klein, W.C. Baird Jr., B.R. Cook, J.G. Chen, S. Hantzer, D.E.W. Vaughan, E.S. Ellis, O.C. Feeley, J. Catal. 210 (2002) 137–148.
- [13] C.A.A. Monteiro, D. Costa, J.L. Zotin, Dilson Cardoso, Fuel 160 (2015) 71–79.
- [14] A. Corma, F. Mocholi, A.V. Orchillés, G.S. Koermer, R.J. Madon, Appl. Catal. A 67 (1991) 307–324.
- [15] J. Abbot, J. Catal. 123 (1990) 383–391.
- [16] D. Kubicka, N. Kumar, P. Maki-Arvela, M. Tiitta, V. Niemi, H. Karhu, T. Salm, D.Y. Murzin, J. Catal. 222 (2004) 65–79.
- [17] D. Kubicka, N. Kumar, P. Maki-Arvela, M. Tiitta, V. Niemi, H. Karhu, T. Salm, D.Y. Murzin, J. Catal. 227 (2004) 313–327.
- [18] R. Moraes, K. Thomas, S. Thomas, S. van Donk, G. Grasso, J.-P. Gilson, M. Houalla, J. Catal. 286 (2012) 62–77.
- [19] M.A. Vicerich, V.M. Benitez, M.A. Sánchez, C.L. Pieck, Catal. Lett. 145 (2015) 910–918.
- [20] M. Daage, J. Santiesteban, XIX Simp. Iber. Catal., Mérida, México, 5/09/2004, plenary lecture.
- [21] D. Santi, T. Holl, V. Calemma, J. Weitkamp, Appl. Catal. A 455 (2013) 46–57.
- [22] H. Kubika, J. Catal. 12 (1968) 223–237.
- [23] M.A. Sánchez, V.A. Mazzieri, M. Oportus, P. Reyes, C.L. Pieck, Catal. Today 213 (2013) 81–86.
- [24] K.R. Sahu, U. De, Thermochimica Acta 589 (2014) 25–30.
- [25] V.S. Braga, J.A. Dias, S.C.L. Dias, J.L. de Macedo, Chem. Mater. 17 (2005) 690–695.
- [26] E.I. Koi, J.G. Weissman, Catal. Today 8 (1990) 27–36.
- [27] V.V. Bhat, A. Rougier, L. Aymard, G.A. Nazri, J.-M. Tarascon, J. Alloys and Compounds 460 (2008) 507–512.
- [28] Y. Liang, H. Zhang, H. Zhong, X. Zhu, Z. Tian, D. Xu, B. Yi, J. Catal. 238 (2006) 468–476.
- [29] S. Guerrero, J.T. Miller, E.E. Wolf, Appl. Catal. A 328 (2007) 27–34.
- [30] V.A. Valles, B.C. Ledesma, L.P. Rivoira, J. Cussa, O.A. Anunziata, A.R. Beltramone, Catal. Today 271 (2016) 140–148.
- [31] W. Chen, S. Chen, J. Mater. Chem. 21 (2011) 9169–9178.
- [32] B.C. Gates, J.R. Katzer, A.G.C. Schuit, Chem. Catal. Processes, McGraw-Hill, New York, 1979.
- [33] N. Tanaka, S. Ogasawara, S. J. Catal. 16 (1970) 157–163.
- [34] N. Tanaka, S. Ogasawara, J. Catal. 16 (1970) 164–172.
- [35] A. Boréave, A. Auroux, C. Guimon, Microporous Mater. 11 (1997) 275–291.
- [36] B. Coq, F. Figueras, J. Catal. 85 (1984) 197–205.
- [37] F.H. Ribeiro, A.L. Bonivardi, C. Kim, G.A. Somorjai, J. Catal. 150 (1994) 186–198.
- [38] P. Biloen, F.M. Duatzenberg, W.M.H. Sachtler, J. Catal. 50 (1977) 77–86.
- [39] M. Ziolk, Catal. Today 78 (2003) 47–64.
- [40] F.B. Passos, D.A.G. Aranda, R.R. Soares, M. Schmal, Catal. Today 43 (1998) 3–9.
- [41] K. Tanabe, Catal. Today 78 (2003) 65–77.
- [42] K. Tanabe, Catal. Today 8 (1990) 1–11.



- [43] F.B. Passos, D.A.G. Aranda, M. Schmal, *Catal. Today* 57 (2000) 283–289.
- [44] T. Hanaoka, K. Takeuchi, T. Matsuzaki, Y. Sugi, *Catal. Today* 8 (1990) 123–132.
- [45] K. Tanabe, *Catal. Today* 78 (2003) 65–77.
- [46] S. Chien, B.N. Shelimov, D.E. Resasco, E.H. Lee, G.L. Haller, *J. Catal.* 77 (1982) 301–303.
- [47] D.A.G. Aranda, F.B. Noronha, M. Schmal, *App. Catal. A* 199 (1993) 77–84.
- [48] S.J. Tauster, S.C. Fung, *J. Catal.* 55 (1978) 29–35.
- [49] J. Zhang, M. Zhang, Z. Jin, J. Wang, Z. Zhang, *Appl. Surf. Sci.* 258 (2012) 3991–3999.
- [50] S. Bernal, J.J. Calvino, M.A. Cauqui, J.M. Gatica, C. López Cartes, J.A. Pérez Omil, J.M. Pintado, *Catal. Today* 77 (2003) 385–406.
- [51] M. Primet, M.E. Azhar, R. Frety, M. Guenin, *Appl. Catal.* 59 (1990) 153–163.
- [52] S.A. D'Ippolito, V.M. Benitez, P. Reyes, M.C. Rangel, C.L. Pieck, *Catal. Today* 172 (2011) 177–182.
- [53] V.M. Benitez, M. Boutzeloit, V.A. Mazzieri, C. Especel, F. Epron, C.R. Vera, P. Marécot, C.L. Pieck, *Appl. Catal. A* 319 (2007) 210–217.
- [54] V.A. Mazzieri, J.M. Grau, J.C. Yori, C.R. Vera, C.L. Pieck, *Appl. Catal. A: Gen.* 354 (2009) 161–168.
- [55] S.A. D'Ippolito, L.B. Gutierrez, C.L. Pieck, *Appl. Catal. A* 445–446 (2012) 195–203.
- [56] M.A. Arribas, P. Concepción, A. Martínez, *Appl. Catal. A* 267 (2004) 111–119.
- [57] A. Corma, B.W. Wojciechowski, *Catal. Rev. Sci. Eng.* 27 (1985) 29–150.
- [58] M. Samoila, V. Boutzeloit, C. D'Ippolito, F. Especel, C.R. Epron, P. Marécot, C.L. Pieck, *Appl. Catal. A* 332 (2007) 37–45.
- [59] M.A. Vicerich, V.M. Benitez, C. Especel, F. Epron, C.L. Pieck, *Appl. Catal. A* 453 (2013) 167–174.